DESIGNCON® 2026
WHERE THE CHIP MEETS THE BOARD

An improved broadband material characterization method

Feng-Nan (Leon), Wu, Samtec

Xingling (Mick), Zhou, Samtec

Tony, Chen, Samtec

Abstract

We propose an enhanced broadband material characterization technique for extracting dielectric constant (Dk) and loss tangent (Df) in high-speed interconnect applications. The method uses two coaxial airlines of different lengths (50 mm and 60 mm), measured with and without the material under test (MUT), combined with Automatic Fixture Removal (AFR) for precise S-parameter de-embedding. This technique avoids reference-plane alignment and physical length dependency by leveraging propagation constant relationships which differ from NRW/NIST approaches. Closed-form equations derived from multilayer lossy coaxial theory eliminate metal loss and geometric tolerances. The Djordjevic–Sarkar model extends bandwidth beyond 40 GHz, validated through 3D-printed HT200 samples and Swissto12 waveguide kit measurements. Results demonstrate accuracy, scalability, and immunity to manufacturing tolerances, enabling future characterization up to 100 GHz and beyond.

Author(s) Biography

Leon Wu has 21 years of industry experience as an SI engineer having worked at FCI, Flextronics and Samtec. He received his Ph.D. from the National Taipei University of Technology in 2013. Leon works in the SI lab at Samtec Taipei and Dongguan facility which focus on connector measurements. He also performs full wave simulations which support research efforts. He has 6 patents related to connector/footprint design.

Xingling (Mick) Zhou received a PhD in electrical engineering with an emphasis in electromagnetic theory and microwave engineering from Arizona State University (ASU) in 2001. He has more than 24 years of experience in EM theory, RF/microwave techniques, and signal integrity designs of IC packaging, interconnects and PCBs, and SI measurement techniques. He has authorized more than 20 journal and conference publications in EM theory, signal integrity, and holds several USA patents. Mick manages an interconnect design hub and global SI labs at Samtec.

Tony Chen has 15 years of industry experience as an SI engineer and SI lab engineer having worked at Inventec, ASMedia, and Samtec. He received his Master's Degree from the National Taipei University of Technology in 2008. Tony works for the SI lab at Samtec Taipei and focuses on RF and connector measurements.

Introduction

As data rates approach 224 Gbps, material characterization accuracy becomes critical for signal integrity and system reliability. Inaccurate characterization may cause design failures since most of the designs start from simulation. An improved method utilizing airline measurements is introduced to accurately and efficiently determine the dielectric constant and loss tangent of a material for broadband applications. This approach surpasses traditional methods like the well-known NRW/ NIST [1],[2] and its iteration versions in precision and efficiency.

Traditional methods, such as NRW and NIST, face practical limitations—require precise reference-plane alignment, iterative calculations, and sensitivity to manufacturing tolerances, which often lead to errors and inefficiencies. For example, the NRW method requires reference planes to align with the sample faces to calculate the correct group delay. This approach works well at off resonance, where the sample length is not a multiple of one-half wavelength in the material. NRW also depends on accurate knowledge of both the sample and airline lengths to rotate the reference planes. In practice, it is difficult to position samples precisely in the airline, especially at low frequencies where the wavelength is long. After calculating reflection and transmission coefficients, permittivity and permeability are derived by dividing the material-under-test (MUT) length. Consequently, any error in the MUT length can cause resonance or lead to inaccurate results. The NIST method introduces an additional iterative process to determine reflection and transmission (T/R) coefficients by solving two equations for the air-section length. However, this approach still incorporates metal loss and geometric factors into the coefficients, limiting its accuracy.

We introduce a propagation-constant-based approach using two coaxial airlines and AFR de-embedding, eliminating dependency on physical length and geometric tolerances. The proposed process employes a de-embedding technique and two airlines with/without MUT method to overcome some mathematical difficulties in the existing methods to precisely determine S-parameters of uniform airlines. It involves measuring two airlines of different lengths (50 mm and 60 mm are used in this paper), both with and without the MUT, which are shaped as hollow cylinders matching the airline shapes and lengths. The Automatic Fixture Removal (AFR) process is then applied to both scenarios to obtain precise S-parameters of two coax lines, effectively eliminating imperfections at the airline ends.

Instead of rotating the reference planes, the transmission and reflection coefficients (both with and without the MUT) can be obtained from the de-embedded S-parameters through the T/R method. The electrical length with and without the MUT is determined by the difference in airline lengths instead of physical length measurement. By using the closed formula for multilayer lossy coax lines[3][4], the physical lengths, metal loss, and geometric size are negated through the derived equations, allowing for the accurate calculation of the dielectric constant and loss tangent of the DUT. This method is independent of metal loss and physical lengths, thereby eliminating errors caused by measurement and manufacturing uncertainties. Since the MUT completely fills out the

space inside the airlines, the airlines with and without MUT are uniform coaxial lines. There are no discontinuities at the reference planes, the resonance issues inherent in the NRW/NIST method are completely avoided.

The method is demonstrated with an experiment. Two Maury 2.92 mm airlines with lengths 50 mm and 60 mm are used to obtain broadband data up to 40 GHz. The MUT is a hollow cylinder, with inner and outer radii of 0.635 mm and 1.46 mm to fit the airlines. The air gap effect is studied and can be compensated for by measuring the physical size of the MUT. Additionally, the Djordjevic-Sarkar (DS) model can be used to extend the bandwidth further as needed. The results are validated by 3D printed HT200 samples through simulations and measurement with commercial waveguide methods (Swissto 12 material characterization kit).

This technique enables accurate characterization up to 40 GHz today and is scalable extension beyond 100 GHz for next-generation interconnects.

Challenges of Nicolson-Ross-Weir (NRW)Solutions

A measurement using an airline involves placing a sample in a section of the airline and then measuring the two-port complex scattering parameters with a vector network analyzer. The reference planes must be the sample faces to calculate the correct group delay as shown in Fig.1.[1],[2].

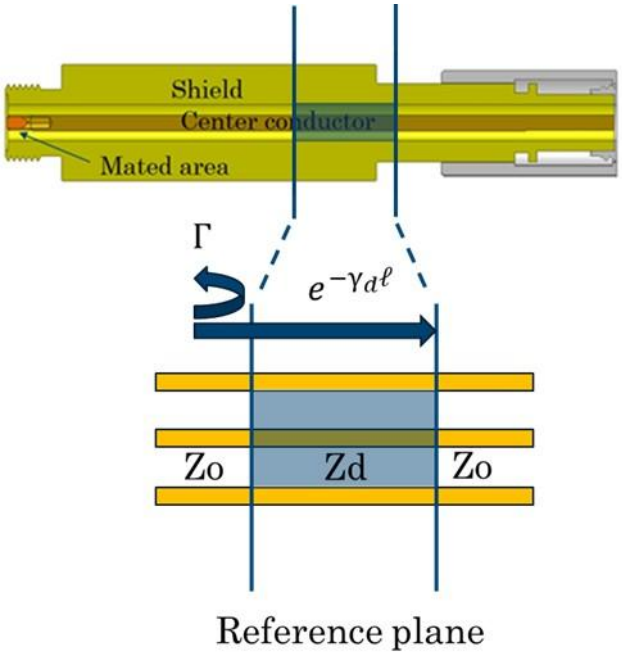

Fig. 1. A dielectric sample in a transmission line; the incident and reflected electric field distributions in the regions Z0, Zd and Z0 are calculated by rotating the reference plane to the faces of dielectric sample.

The reflection coefficient, Γ and transmission coefficient, $e^{-\gamma_d \ell}$ can be calculated by multiple reflection/transmission and expressed by S-parameters [1]:

$$X = \frac{(S_{11}^2 - S_{21}^2) + 1}{2S_{11}} \quad (1)$$

$$\Gamma = X \pm \sqrt{X^2 - 1} \quad (2)$$

where the correct root must satisfy | Γ |<=1, then the transmission coefficient can be obtained by:

$$Z_1 = e^{-\gamma_d \ell} = \frac{(S_{11} + S_{21}) - \Gamma}{1 + (S_{11} + S_{21})\Gamma} \quad (3)$$

By letting:

$$\frac{1}{\Lambda^2} = -\left[\frac{1}{2\pi\ell} ln\left(\frac{1}{Z_1}\right)\right]^2 \quad (4)$$

The permeability can be calculated:

$$\mu_R = \frac{1+\Gamma}{(1-\Gamma)\Lambda\sqrt{\frac{1}{\lambda_o^2} - \frac{1}{\lambda_c^2}}} \quad (5)$$

Where λ_o is the free space wavelength and λ_c is the cutoff wavelength, which is infinite for a coaxial line.
The permittivity is:

$$\epsilon_R = \frac{\lambda_o^2}{\mu_R}\left[\frac{1}{\lambda_c^2} + \frac{1}{\Lambda^2}\right] \quad (6)$$

Rotating the reference planes to align with the faces of the dielectric sample is challenging and often results in the sample length that either includes an air section or is shorter than the original sample length. The NIST method addresses this by adding airline sections into the calculation; however, it requires an initial guess of the material properties, and the computed values may fail to converge at certain frequency points. The air-section effect in NRW can be evaluated using a 3D commercial simulation tool by adding air gaps of 0.005 mm, 0.01 mm, and 0.015 mm before a 10 mm dielectric sample. These added lengths correspond to 0.05%, 0.1%, and 0.15% of the MUT length. The typical length tolerance between the center conductor and outer conductor in a coaxial airline is about 0.0127 mm, and when combined with MUT tolerances, the

variation can easily exceed 0.015 mm. The results are highly sensitive to the sample length, ℓ as shown in (3).

For simulation, the input dielectric constant and loss tangent are set to 3 and 0.02 using the Djordjevic–Sarkar model at 1 GHz, as shown by the black line in Fig. 2. The simulated S-parameters are overlapped. By applying equation (6), the dielectric constant and loss tangent can be extracted, as shown in Fig. 2. The results indicate that longer air sections produce stronger resonance. Comparing low- and high-frequency regions in Fig. 2(a) and (b), the resonance at low frequency is sharper because the added air section is relatively long compared to the wavelength.

It should be noted that conductivity, plating permeability, and size were not considered in equations (1) – (6); these factors are inherently included in the measured S-parameters. Consequently, the extracted dielectric constant and loss tangent reflect these combined effects.

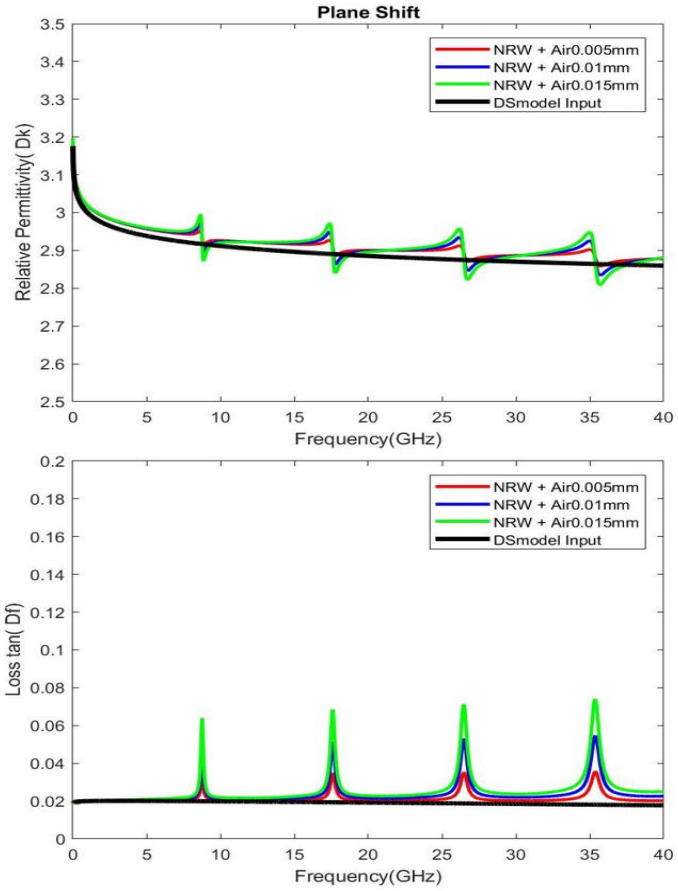

Fig. 2. The extracted permittivity (a, above) and loss tangent (b, below) from adding the air section are shown. The resonance frequencies observed in (a) and (b) correspond to multiples of the sample's one-half wavelength.

In [2, Ch. 2.1.2], imperfection factors related to sample inhomogeneity are discussed. A similar phenomenon occurs when the sample faces are not perfectly orthogonal to the airline axis. Ideally, γ should be independent of transverse coordinates, and the eigenfunctions for transverse components in the air and sample regions should satisfy an

orthogonality condition. In such cases, mode-by-mode matching is possible, and the coefficients are decoupled.

However, due to manufacturing tolerances, the sample faces cannot be perfectly orthogonal to the airline axis and may even include small air gaps near the faces. Fig. 3 shows the E/H field distribution when the sample faces are rotated by approximately 0.034° at 11 GHz. The field is no longer uniform around the center conductor, which further reduces the accuracy of the de-embedded S-parameters.

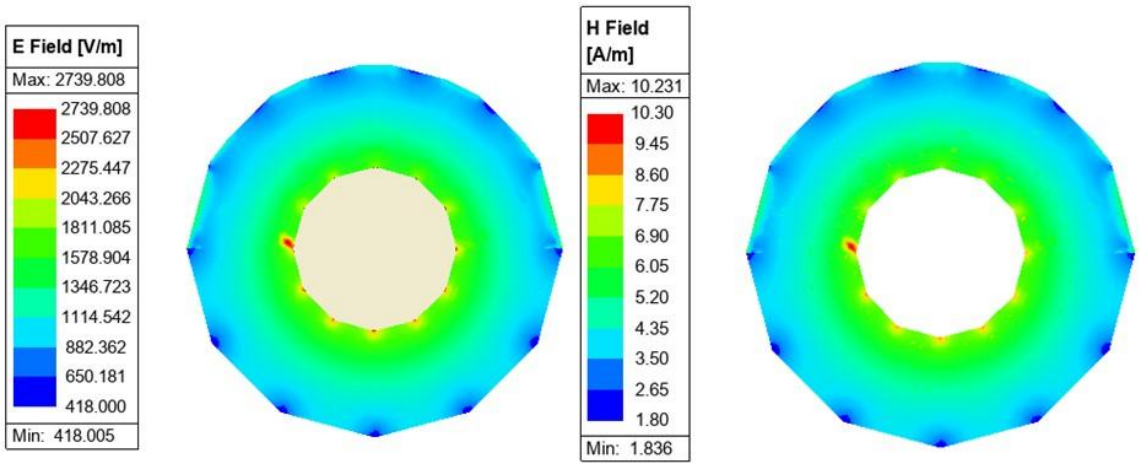

Fig. 3. E/H field distribution when the sample faces are rotated by approximately 0.034° at 11 GHz. The non-uniform field around the center conductor illustrates how slight misalignment of sample faces.

The impacts on the resonance of the extracted dielectric constant and the tangent loss are like the adding air section shown in Fig.2.

The improved method: Theory, Simulation, and Imperfections

In [3][4], a general first-order approximation of the propagation constant is derived based on rigorous field analysis, considering different conductivity and permeability in the regions of a coaxial airline. This theory forms the basis of our equivalent method.

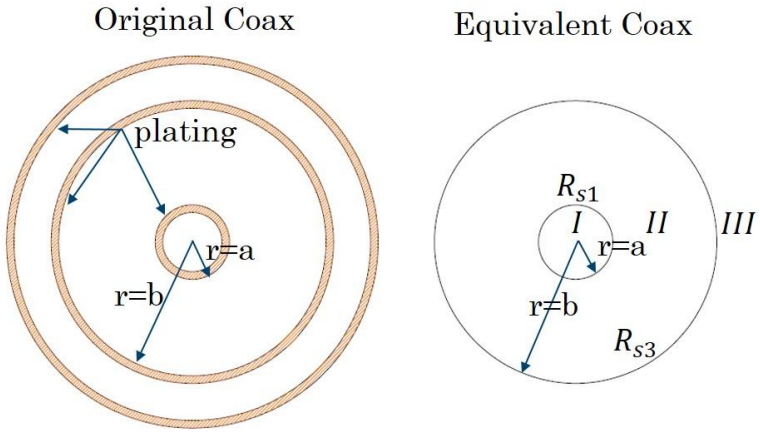

Fig.4 Cross section of a coax airline showing 3 regions: (I) r< a, (II) b> r > a, air or dielectric. (III) r> b, outer shield. The equivalent model simplifies complex plating.

Fig.4 illustrates the original problem and its equivalent. The inner radius after plating of outer conductor is b, and the outer radius of inner conductor after plating is a. In the original problem, the shield and center pins have different plating and may be multiple plating layers. Obtaining an analytical solution for this multilayer structure is computationally challenging, even numerically in model simulation tools. However, if we assume its equivalent problem on the right exists, which has the same propagation constant, an analytical solution can be employed for our purpose.
For the equivalent problem, the propagation constant is given in [3][4] as:

$$\gamma = (h^2 - k_2^2)^{1/2} = jk_2\left(1 - \frac{h^2}{k_2^2}\right)^{1/2} \tag{7}$$

Where $k_2 = \omega\sqrt{\mu_2\varepsilon_2}$ is wave number in region II ($a \le r \le b$), h is a separation constant; Under the microwave approximation (MA), h=h0, (7) is simplified in [4] as:

$$\frac{h_0^2}{k_2^2} = \frac{j(\frac{\mu_1}{ak_1} + \frac{\mu_3}{bk_3})}{\mu_2 ln\,(\frac{b}{a})} \tag{8}$$

It should be noted there is a cutoff point of the approximation in (8). In [4], the author indicated the point at about 1MHz for a 7 mm line.

$$k_i = \sqrt{\omega\mu_i\sigma_i}e^{-j\pi/4}\,,\ i = 1,3 \tag{9}$$

With small h compared to 1; (7), (8), (9) can be expressed as

$$\hat{\gamma} = k_2\frac{(\frac{1}{a}\sqrt{\frac{\mu_1}{\sigma_1}} + \frac{1}{b}\sqrt{\frac{\mu_3}{\sigma_3}})}{2\sqrt{2\omega}\mu_2 \ln\,(\frac{b}{a})} + jk_2\left[1 + \frac{(\frac{1}{a}\sqrt{\frac{\mu_1}{\sigma_1}} + \frac{1}{b}\sqrt{\frac{\mu_3}{\sigma_3}})}{2\sqrt{2\omega}\mu_2 \ln\,(\frac{b}{a})}\right] = \alpha + j\beta \tag{10}$$

From (10), compared to (3) and (4), it is straightforward that the propagation constant depends on the conductivity and permeability of the center conductor and shield, as well as the dimensions (a,b), and therefore affects the extracted dielectric constant and loss tangent. To simplify the problem, by considering the metal used in (10) to perfect conductors, then (10) becomes:

$$\hat{\gamma}_{d_{PEC}} = jk_d = \alpha_{dPEC} + j\beta_{dPEC} \tag{11}$$

where $k_d = \omega\sqrt{\mu_o\epsilon_o}\sqrt{\epsilon_R(1 - jtan\delta)}$ and α_{oPEC}~0 while α_{dPEC} caused by the loss tangent which means $\hat{\gamma}_{dPEC}$ is metal loss and geometric independent. To compare the impacts, the attenuation constant α and β phase constant were plotted in Fig.5. The center conductor and shield are set to gold (conductivity 4×10^7 S/m) and use a 2.92 mm interface with a=0.635 mm and b=1.46 mm. The permeability is set to 1 for the conductors, and the length is set to 10 mm. The dielectric constant and loss tangent were set to 3 and 0.02 at 1 GHz using the Djordjevic-Sarkar (DS) model. From Fig. 5, $\alpha\ell$ has greater impacts than $\beta\ell$, which is expected since gold has high conductivity but is not a perfect conductor, PEC. Conductor loss is not a major factor if good conductor material is

used. The propagation speed in the airline is primarily determined by the dielectric material, not metal loss, unless weak magnetic plating is used, as noted in [5][6].

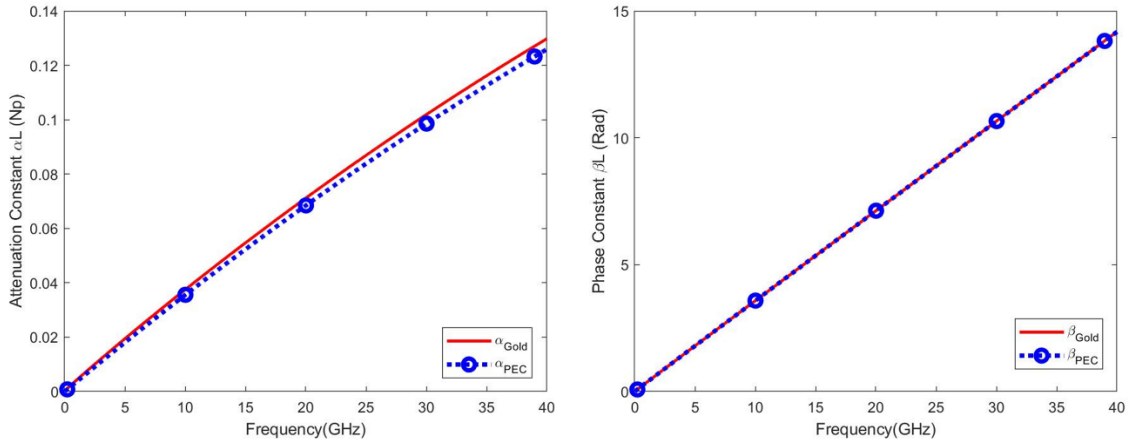

Fig.5 Comparison of attenuation constant (α) and phase constant (β) for a 2.92 mm interface using gold conductors and a dielectric with Dk=3 and Df=0.02. α_{dPEC} caused only by the loss tangent, whereas α_{Gold} includes both conductor loss and loss tangent.

It is noted the 2.92 mm interface is capable up to 40 GHz due to the limitation of high order mode. If the required bandwidth increased, then the different decreased size of airline should be used.

From (10), the attenuation constant α and β phase constant are functions of radius a and b. Common airline sizes such as 2.92 mm, 1.85 mm, and 1 mm were studied to evaluate these impacts. The $\frac{b}{a}$ used here is approximately 2.92/ 1.27. The radius of center conductor, a, equals 0.635 mm, 0.40 mm, and 0.22 mm, respectively. The attenuation constant is plotted below. Smaller sizes result in larger attenuation constants. The dielectric constant and loss tangent can be extracted using the NRW method under ideal conditions, i.e., no air gaps and perfectly aligned reference planes. As shown in Fig. 6, the dielectric constant varies slightly between sizes, indicating that the extracted value is not completely size-independent. In addition, we found that if $\frac{b}{a}$ remains constant, then the extracted values are similar. However, this is impractical because tolerances vary between interfaces and manufacturers.

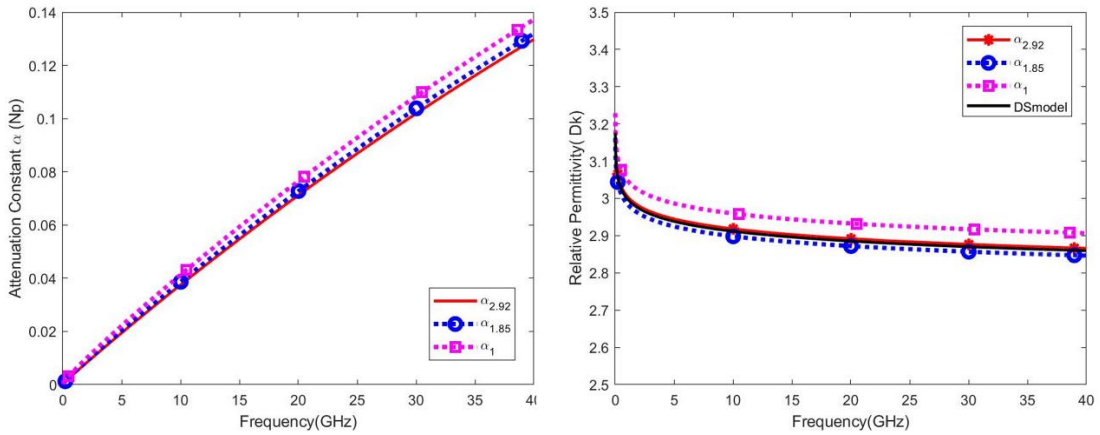

Fig.6 (a) Comparison of attenuation constant (α) for different interfaces based on equation (10). (b) Extraction of the dielectric constant (Dk) for different interfaces using the NRW method.

Corrected propagation constant

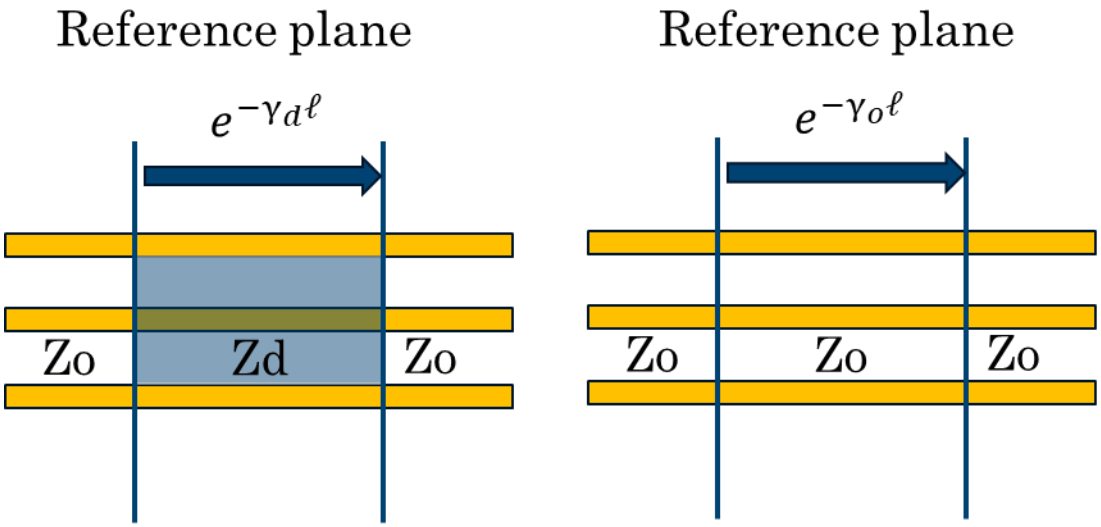

Fig.7 Additional measurements on the airline itself, without a filled dielectric, can be performed directly (left), compared to the NRW setup (right).

Additional measurements can be performed so that the conductivity, permeability, and geometric information contained in (10) can be obtained. In this case, the propagation constant in the airline filled with air equals to $\hat{\gamma}_o = \alpha_0 + j\beta_0$, and when filled with MUT, it equals $\hat{\gamma}_d = \alpha_d + j\beta_d$. Assuming the relative permeability equals 1, then the relationship between two conditions is:

$$\hat{\gamma}_d \ell = \sqrt{\varepsilon_r}(\alpha_0 \ell + \frac{1}{2} tan\delta \beta_0 \ell) + j\sqrt{\varepsilon_r}(\beta_0 \ell - \frac{1}{2} tan\delta \alpha_0 \ell) \quad (12)$$

Where $k_d = k_0\sqrt{\varepsilon_r(1-jtan\delta)} \sim k_0\sqrt{\varepsilon_r}\left(1-j\frac{1}{2}tan\delta\right)$ in (10). By introducing:

$$\mathcal{R} = \frac{\beta_d \ell}{\alpha_d \ell} = \frac{\beta_0 \ell - \frac{1}{2}\alpha_0 \ell(tan\delta)}{\alpha_0 \ell + \frac{1}{2}\beta_0 \ell(tan\delta)} \tag{13}$$

$$tan\delta = \frac{2(\beta_0 \ell - \mathcal{R}\alpha_0 \ell)}{\alpha_0 \ell + \mathcal{R}\beta_0 \ell} \tag{14}$$

$$\sqrt{\varepsilon_r} = \frac{\alpha_d \ell}{\alpha_0 \ell + \frac{1}{2}\beta_0 \ell(tan\delta)} \tag{15}$$

From (14) and (15), the obtained dielectric constant and loss tangent are independent of MUT length, geometric variations, and conductor properties. Thus, even if the airline geometry contains tolerances across different interfaces, equations (14) and (15) remain valid. The dielectric and loss tangent for the three interfaces studied in Fig.7 were re-extracted using (14) and (15). The results show that the extracted values overlap, as illustrated in Fig. 8, confirming that the method is robust against geometric and conductivity variations.

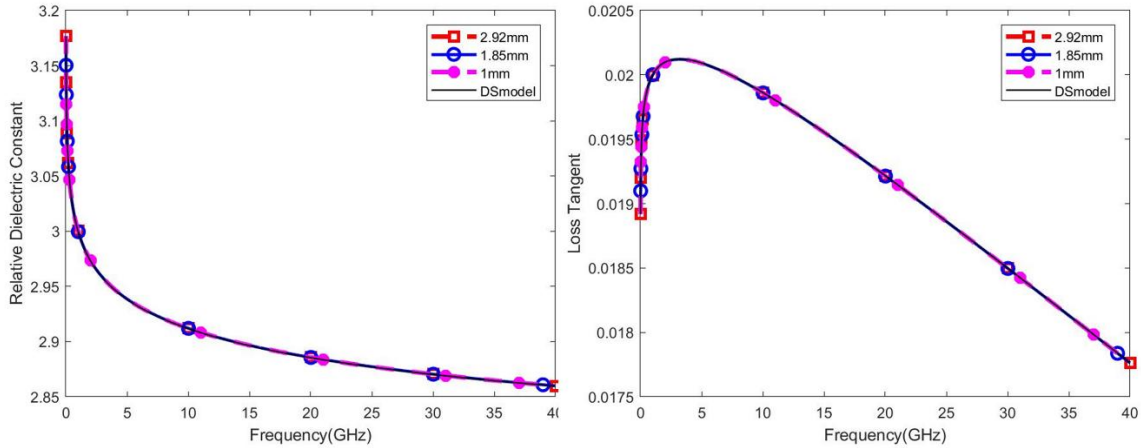

Fig.8 The extracted dielectric constant and loss tangent are independent from different interface, conductor properties, and the length of MUT.

Time-Domain Gating in the Improved Method

In the NRW method, rotating the reference plane to align with the faces of dielectric samples is challenging. The time-domain gating approach addresses this by using the time-domain reflectometry (TDR) waveform of the thru standard through one-half of its length, which accurately captures the reflection information for that section [7–10]. Thus, even in an asymmetric fixture, it is still able to extract the reflection. Furthermore, an impedance-corrected de-embedding method can remove reflections and mismatches caused by a nonideal fixture [11][12].

Consider two coaxial airlines of different lengths that share the same center and outer conductor radii and follow a similar process, meaning their tolerances and plating are comparable, as shown in Fig. 9.

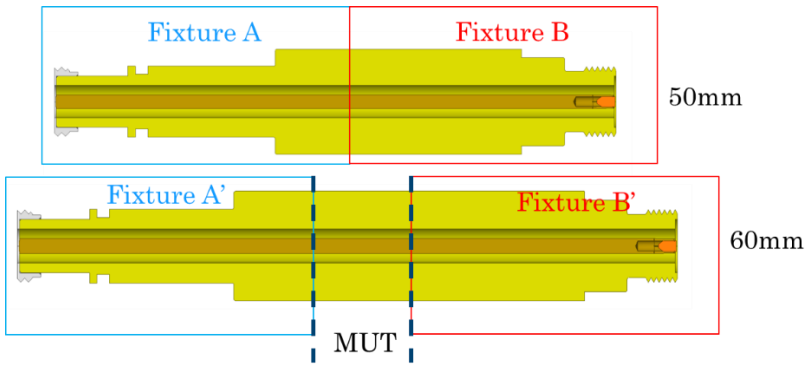

Fig.9 The setup of time domain gating method. The 50 mm airline works as a 2X thru(above). The fixture-DUT-fixture, 60 mm.

The time-domain gating method is then applied to remove Fixture A' and Fixture B'. Note that the lengths in Fig. 9. from with/without MUT measurements are identical. To achieve this, two different airline lengths are used in the study; first, 50 mm and 60 mm long airlines are measured without MUT to obtain the propagation constant, $\hat{\gamma}_0 \ell$ where the ℓ is the length difference approximately 10 mm. The MUT is then placed between the fixtures. However, accurately positioning the MUT in the middle is difficult, as noted in the NRW section. Even if the MUT is centered, significant reflections occur between the air and MUT sections. To evaluate these impacts, an air section is added as in the NIST system to complete the equations, but it is still difficult to extract the Dk and Df across a broadband range.

In this study, we propose filling the entire airline with dielectric material so that the interface is continuous and the MUT is naturally located in the middle of the 60 mm airline. This reduces reflections to those between the cable and Fixture A/B, which can be handled through proper renormalization.

It is also important to consider size differences between the two airlines due to tolerances, meaning the radii a and b for the 50 mm and 60 mm airlines may differ slightly. Using (10) with a 2.92 mm interface (i.e. a=0.635 and b=1.46 mm), the center conductor and shield are set to gold (conductivity 4 x 10^7 S/m). The same Djordjevic-Sarkar model is applied for the dielectric, with lengths set to 50 mm and 60 mm. The tolerance is ±0.005 mm, with a variance from 0.63 to 0.64 mm and b varies from 1.455 to 1.465 mm. The propagation constants, $\hat{\gamma}_0 \ell$ and $\hat{\gamma}_d \ell$ with different tolerance are obtained. The real parts of Z0 with and without dielectric at 5 GHz vary from 49.6 to 50.6 ohm and 28.7 to 29.5 ohm, respectively. The calibration bandwidth for 50 mm airline itself is greater than 40 GHz through the theoretical line (10), and the separation between insertion loss (IL) and return loss (RL) is greater than 25 dB with the tolerances. However, when the dielectric is inserted, RL increases significantly due to the impedance changes, though the bandwidth remains supported; the separation is about 5 dB as shown

in Fig.10. If the dielectric constant further increased to 4, the separation drops below 1 dB. In Fig. 10, there are four groups of data: the dotted lines represent IL (red) and RL (blue) without the dielectric, while the solid lines represent IL (red) and RL (blue) with the dielectric. All groups account for tolerance.

To improve the bandwidth of the 2X thru with dielectric, several methods can be applied:
1. Use a high impedance airline so that the impedance decreases after the dielectric insertion, since the proposed method is independent of geometric/ impedance.
2. Apply proper re-normalization.
3. Use short airlines. In the study, 50 mm and 60 mm airlines are used, but shorter length is also feasible.

Finally, the separation rule is not a necessary condition when using an impedance-corrected method such as AFR (Auto Fixture removal) and ISD. For most material used in the cable/connector industry, the dielectric constant is smaller than 4.x, so a 50 Ohm airline is sufficient for measurement.

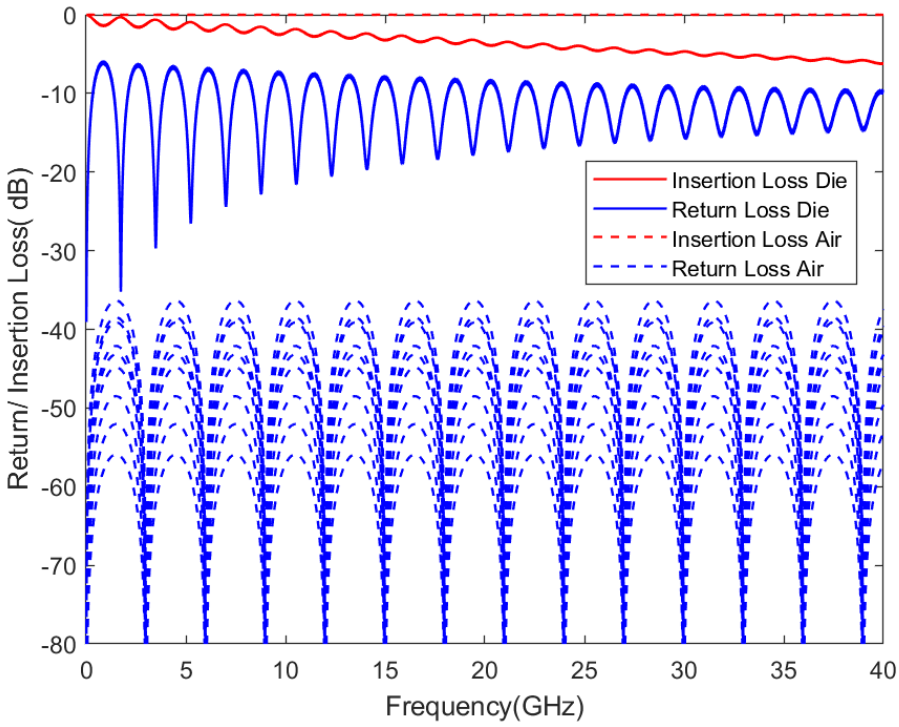

Fig.10 The separation between return and insertion loss with/without the dielectric filled into the airlines.

After applying the IEEE P370 time gating method [10] for de-embedding, the dielectric constant and loss tangent can be extracted (Fig. 11). In total, there are 81 cases, but only 73 curves appear because changes in a, b are identical in both 50 mm and 60 mm airlines, making the results geometry-independent per (14) and (15). If the changes differ slightly between the two airlines, the variations in extracted dielectric constant and loss tangent

remain small. The red dotted line shows the input from the Djordjevic–Sarkar model in (10).

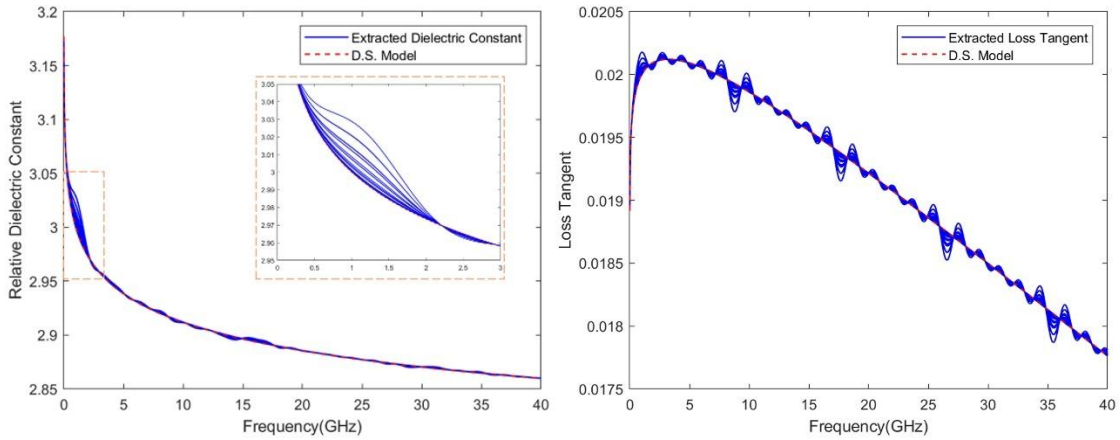

Fig.11 The extracted dielectric constant and loss tangent utilized (14) and (15) from the IEEE P370 de-embedded S parameters.

Through (6), the impacts of the NRW method and the setup shown in Fig. 12 are studied. Tolerances in a and b directly affect Dk and Df, causing significant errors. From (1)-(3), it is straightforward to calculate the transmission and reflection coefficients. However, any small error in these equations is treated as part of the MUT, significantly altering the extracted values. In our proposed method, errors in the propagation constant caused by imperfections are minimized, as shown previously in Fig. 11, and are effectively canceled during the extraction of the material's dielectric constant (Dk) and loss tangent (Df).

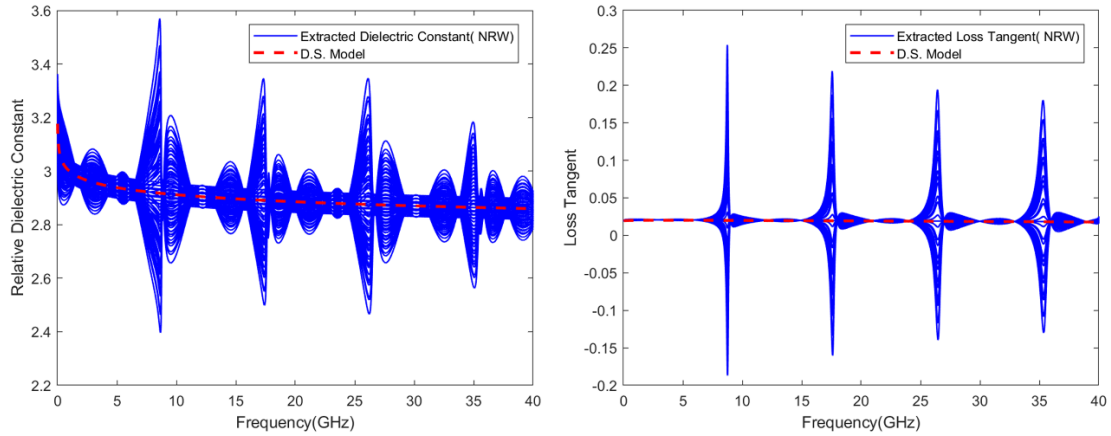

Fig.12 The extracted dielectric constant and loss tangent utilized NRW(1)-(6) from the IEEE P370 de-embedded S parameters.

Practical Issue and Optimization

It may not be practical to assume an ideal coax line for real-world cases. For example, modeling a MUT with a hollow shape as long as 50 mm or 60 mm in a 2.92 mm interface structure with different sections using (10) is challenging. The dielectric samples with such long lengths are also difficult to manufacture. Additionally, the initial assumption of

the time-gating method [7] presumes the 2x thru must be symmetrical, meaning the insertion loss of S12A equals S12B, which requires both fixtures to have the same gender. This is an option that is not readily available on the market. The geometry of the female side is complex and difficult to model as an ideal coaxial line. In practical cases, if the shape of MUT can be properly designed so that S12A and S12B can be close enough, the accuracy improves. On the male side, the dielectric can be designed to be uniform along the Z-axis. However, the female side must account for the contact size after mating with the male-side cable/adapter, as shown in Fig. 13. The hole in the dielectric for female side is determined by the inner radius and the spring length of the center conductor.

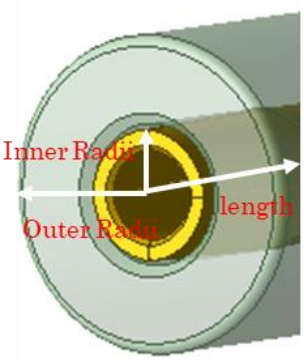

Fig. 13 The dielectric shape for the female side of a center conductor.

Since the adapter male pin is solid, the minimum inner radius on the female side cannot be smaller than the mated radius of center conductors, or it would collapse the airline. Additionally, the mated interfaces of cable assemblies and adapters have manufacturing tolerances. Therefore, we limited the minimum radius of the dielectric to meet the time-gating method assumptions.

To evaluate these impacts, we used a commercial 3D modeling tool (HFSS) to analyze two different genders on the coaxial airline with dielectric filling and to check the group delay and magnitude of S12 for both sides. First, we began with the female side and performed a DOE analysis using the Modified Hausdorff Distance (MHD) [13] value. The MHD calculated the minimum distance from the real and imaginary parts. To find the optimized design value within an increasing range, we input the following parameters in HFSS: the inner radius and the length of the hole in the dielectric (considering the size of the center conductor but not tolerances). This approach identifies whether the optimized design value is bounded by physical limitations. The MHD value should be as small as possible, indicating similarity between the two datasets. We set the male side as the reference and vary the female side. For the length of hole inside the dielectric, the optimal length is found to be around 1.95-2 mm, as these values yield smaller MHD compared to 1.9 and 2.05 mm, as shown in Fig. 14(a). In Fig.14 (b), the trend indicates that the radius should be as small as possible, which makes sense since the hole in the male side is 0.635 mm. However, the inner radius of the dielectric is limited by tolerance, so we can only select the minimum value, 0.65 mm.

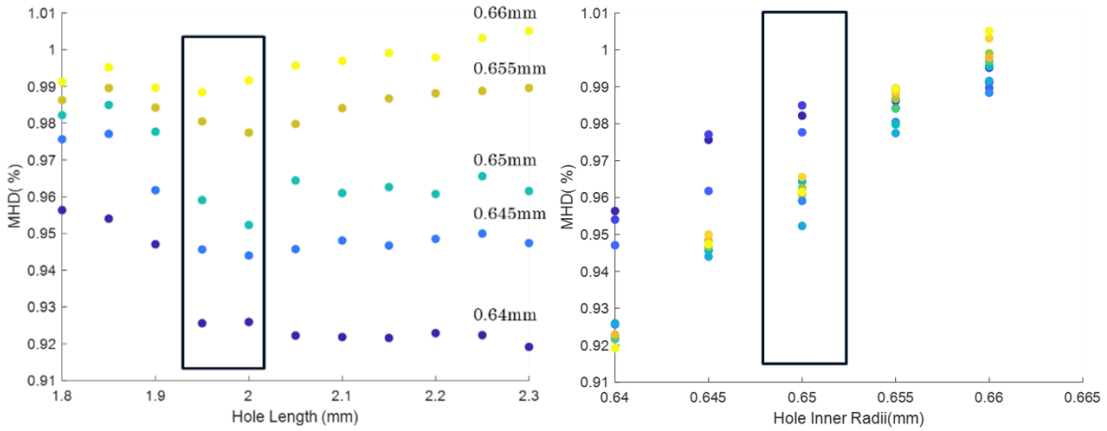

Fig. 14 The MHD values from DOE method varied by different inner radii and length of a female center conductor hole in the dielectric. The same color is used to highlight the same radius.

To overcome the manufacturing issues previously mentioned, the dielectric is separated into two parts; 15 mm with 35 mm and 15 mm with 45 mm. Chamfers are added on the male side to further decrease the MHD values.

Impedance or geometry may vary on the fixture and fixture-DUT-fixture configurations. Tools such as AFR and ISD offer the options to compensate for these differences, but their algorithms are not disclosed. Some studies were discussed in [11][12] about impedance correction by calculating the propagation constant using a 2X thru kit and then, adjusting to the characteristic impedance to match the fixture-DUT-fixture with different normalization methods, reducing the reflection caused by the impedance difference between 2X thru and the fixture-DUT-fixture.

We compared the extracted Dk and Df results using the IEEE P370 scripts and AFR in Fig.15. The dielectric constants match well in all cases, but the loss tangents show difference. These differences are recorded in Table 1 as percentage values compared to the Djordjevic-Sarkar model at different frequencies. It should be noted that the IEEE P370 method used interpolation to calculate DC values and that (10) contained limitations based on wavelength assumptions. To illustrate the S12A= S12B issue, simulation of the same gender (male-male) configurations is added to the results.

We also compared AFR to IEEE P370 in the female-male case. AFR provides closer Dk values at low frequencies up to ~15 GHz as shown in Fig. 15(a) where the Df is closer, but it differs by about 2.61% at 90 MHz, while IEEE P370 differs by about 18% at 2.55 GHz. The low-frequency difference in Df is due to impedance mismatch at the adapter-airline interface. IEEE P370 overlays the input Djordjevic-Sarkar model in the male-male configuration; performing well for both Dk and Df when S12A = S12B. AFR is slightly off below 1 GHz. The difference can be significantly reduced by adding chamfers to the separated two sections in the IEEE P370 method compared to the male-female setting, as S12A is closer to S12B. These improvements reduce discrepancies but remain like AFR.

Freq.(GHz) / Gender	0.09	2.55	8.78	15	20	30	40
IEEE P370 Male-Female(%)	0.85	18.18	13.69	3.37	1.68	0.51	0.77
AFR Male-Female(%)	2.61	1.09	4.09	0.57	0.06	0.33	0.13
IEEE P370 Male-Male(%)	0.03	0.02	0.01	0.02	0.02	0.01	0.01
AFR Male-Male(%)	6.72	0.11	0.33	0.10	0.11	0.07	0.10
IEEE P370 Male-Female 2 Sections(%)	0.24	1.70	0.05	0.49	0.01	0.01	0.03
AFR Male-Female 2 Sections(%)	3.94	0.58	0.34	0.13	0.01	0.05	0.04

Table 1. Percentage errors of different de-embedding methods vs. gender, and dielectric design of an airline.

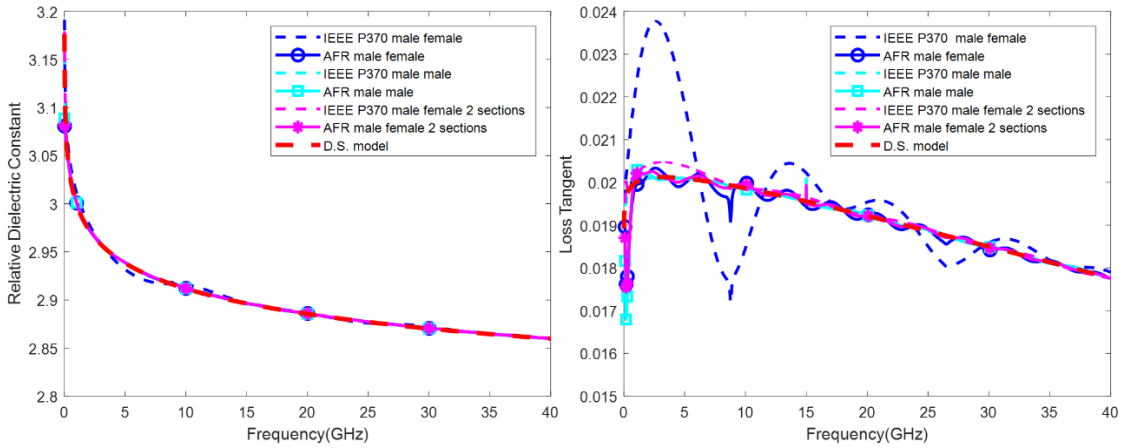

Fig. 15 The extracted dielectric constant and loss tangent from different de-embedding methods, gender, and dielectric design of an airline.

Experiments

Dk and Df correction

In the experiment, 3D-printed HT200 samples are used as MUTs. The dimensions of these samples may include tolerance. Some correction methods based on a capacitance model have been discussed in [2] and [14] to compensate for these tolerances. By calculating the radii of the center line, dielectric, and outer conductor, we can obtain the corrected capacitance. Because the inner radius of dielectric has much more impact than the outer radius, the inner radius must be well controlled. The printed inner radii of the dielectric samples were measured using pin gage, and the measured values are slightly less than the design 0.635 mm which are in the range of 0.63 mm - 0.635 mm. The outer

radius of dielectric measured in the range of 1.453-1.455 mm. Fig. 16 uses the correction method to evaluate the impacts of dielectric geometric variations. The Djordjevic-Sarkar model used in previous section provided the input data, and we calculated the corrected values. The absolute different values are smaller in low frequency and become constant after 5 GHz. However, the percentage difference is 1.2% and 0.8% for Dk at 1 GHz; 2.9% and 2% for Df. And 1.1% and 0.8% for Dk at 10 GHz; 2.8% and 2% for Df. With this level of difference, the tolerance can be ignored.

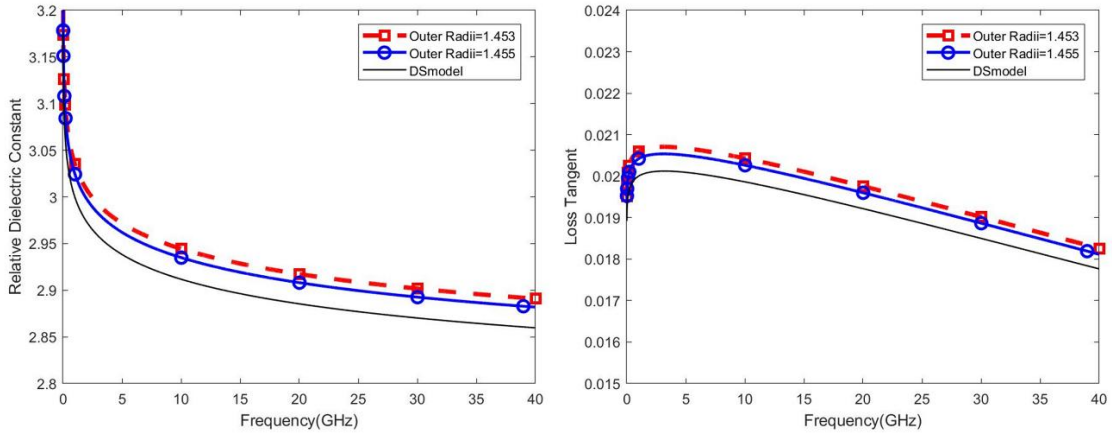

Fig. 16 Impacts of the dielectric samples with manufacture tolerance. The difference is 1.1% and 0.8% for Dk at 10 GHz; 2.8% and 2% for Df at 10 GHz.

It is important to note that the dielectric might not be fully filled to the airline, especially in cases where it needs to be installed by hand with a tight tolerance. Thus, we heated the dielectric to temporarily increase the hole size and fill the center conductor. Then, after they returned to room temperature, we installed them into the airline as shown in Fig 17.

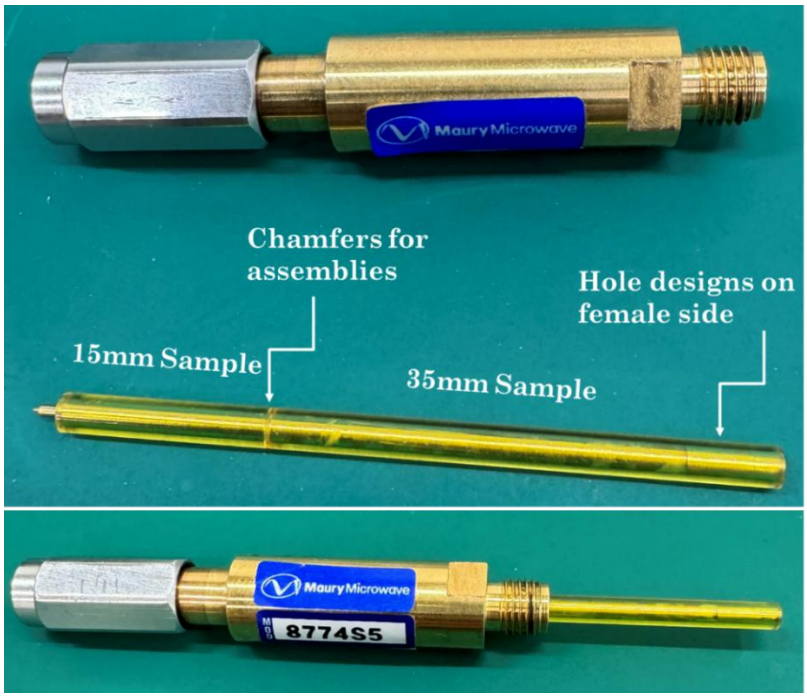

Fig. 17 The center conductor is inserted into the dielectric sample first and then assembled into the outer conductor.

Correlations

To evaluate the accuracy of the proposed characterization method, we fabricated additional samples using HT-200 material and measured with a Swissto12 Material Characterization Kit (MCK) in a waveguide setup. In this study, the printed samples were placed at the center between the waveguides, as shown in Fig. 18. The MCK includes three waveguides for different frequency bandwidths from 26 GHz to 106 GHz.

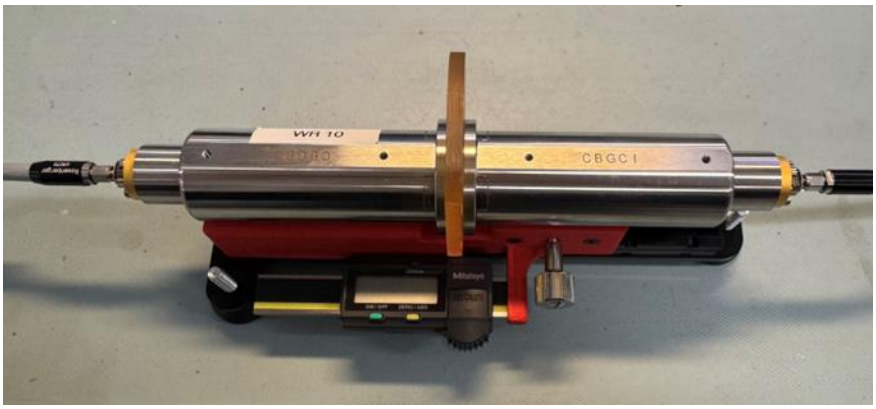

Fig. 18 The Swissto12 Material Characterization Kit with MUT in the middle.

The bandwidth of the 2.92 mm coaxial airline is approximately 40 GHz, which overlaps with the 26–40 GHz of the MCK kit.

To correlate the extracted Dk and Df with the higher-bandwidth MCK measurements, we applied the Djordjevic-Sarkar model to fit the extracted Dk and Df values up to 40 GHz using 1 GHz measurement settings. This method is commonly used in PCB material datasheets and software settings. We then extrapolated to 106 GHz, as illustrated in Fig. 19. The blue square markers represent reference data for HT-200 from the manufacturer's website [15]. The solid red line shows the extracted values from the proposed method without any geometric corrections, while the solid green line represents average data obtained from the Swissto12 MCK measurements. The solid purple and light blue lines represent the tolerances added through compensation from the improved method, which should be negligible. The extracted Df from the coaxial airline measurements deviates slightly compared to the Djordjevic-Sarkar model (up to few hundred MHz), primarily due to impedance mismatches at the VNA ports. However, this level of accuracy is sufficient for most connector and cable applications, where conductor loss dominates over dielectric loss within the application bandwidth.

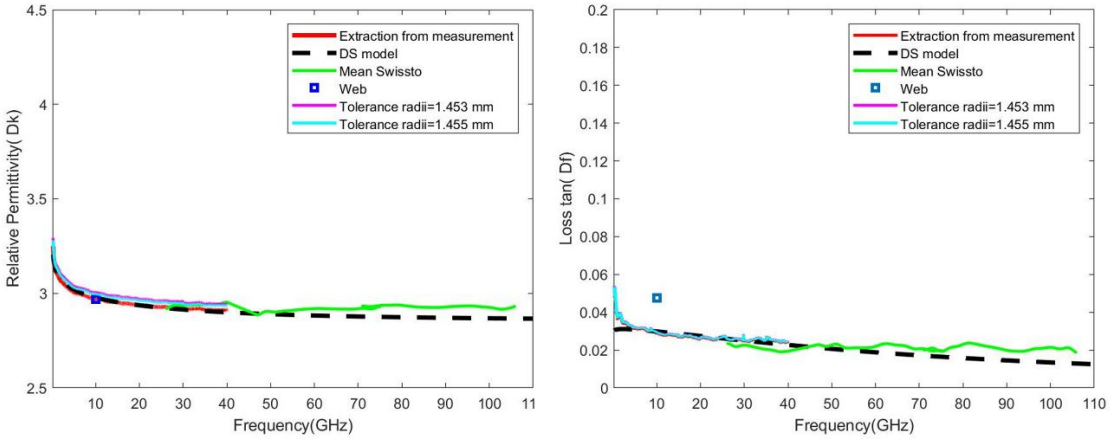

Fig.19 The Dk and Df of the proposed method, Swissto12 MCK, D.S. model and the data sheet values.

Conclusions

This study introduces an improved broadband material characterization method that overcomes key limitations of traditional NRW/NIST techniques. By employing two coaxial airlines of different lengths (50 mm and 60 mm) and applying Automatic Fixture Removal (AFR), the proposed method accurately extracts dielectric constant (Dk) and loss tangent (Df) without relying on precise physical length measurements or reference-plane alignment. The closed-form equations derived of the multilayer lossy coaxial theory significantly reduce dependencies on metal loss and geometric tolerances, ensuring robustness against manufacturing variations.

The method leverages propagation constant relationships, making the extracted parameters largely independent of airline size, conductor conductivity, and MUT positioning after proper de-embedding and normalization. Experimental validation using 3D-printed HT200 samples and Swissto12 waveguide kit measurements confirm accuracy up to 40 GHz, with bandwidth extension beyond 100 GHz achievable through the Djordjevic-Sarkar model. Error analysis demonstrates immunity to tolerance-induced variations, with differences in Dk and Df limited to approximately 1.2% and 2.9%, respectively, well within acceptable margins for high-speed interconnect designs.

Practical considerations, such as impedance mismatch and fixture asymmetry, were addressed through optimized dielectric design and impedance-corrected de-embedding techniques. Comparisons between AFR and IEEE P370 methods show consistent extraction of Dk, while minor discrepancies in Df at low frequencies highlight the importance of proper normalization and fixture design.

This technique provides a scalable, efficient, and highly accurate solution for broadband material characterization, enabling reliable modeling for next-generation interconnects operating at 112 Gbps, 224 Gbps, and beyond. Its independence from physical length and geometric tolerances positions it as a superior alternative to conventional methods. In theory, the method can be extended to other areas, such as high-speed cable material characterization.

References

[1] B.-J. James, J. M. Dunsmore, G. J. H. Jr., and G. R. G., “Transmission/Reflection and Short-Circuit Line Methods for Measuring Permittivity and Permeability,” National Institute of Standards and Technology (NIST), Washington, DC, Dec. 1993, ch. 2.
[2] Rohde & Schwarz, “Measurement of Dielectric Material Properties Application Note,” Available: www.rohde-schwarz.com. [Accessed: Nov. 2025].
[3] W. C. Daywitt, “First-Order Symmetric Modes for a Slightly Lossy Coaxial Transmission Line,” IEEE Transactions on Microwave Theory and Techniques, vol. 38, no. 11, Nov. 1990.
[4] W. C. Daywitt, “Extract Principal Mode Field for a Lossy Coaxial Line,” IEEE Transactions on Microwave Theory and Techniques, vol. 39, no. 8, Aug. 1991.
[5] F.-N. Wu, X.-L. Zhou, and T. Chen, “Accurate Correlation Between SI Simulation and Measurement in High-Speed Backplane Connector Designs,” in Proc. DesignCon, Santa Clara, CA, 2022.
[6] Y. Shlepnev, S. McMorrow, “Nickel Characterization for Interconnect Analysis,” in Proc. IEEE Int. Symp. on Electromagnetic Compatibility (ISEC), 2011.
[7] J. Dunsmore, N. Cheng, and Y.-X. Zhang, “Characterization of Asymmetric Fixtures with a Two-Gate Approach,” in Proc. ARFTG Conf. on Microwave Measurement, Baltimore, MD, Jun. 2011.
[8] Y. Chen, J. He, R. Zai, J. Fan, and J. Drewniak, “De-Embedding Comparisons of 1X-Reflect SFD, 1-Port AFR, and 2X-Thru SFD,” in Proc. Asia-Pacific EMC Symposium (APEMC), Singapore, May 2018.
[9] C. Wu, B. Chen, T. Mikheil, J. Fan, and X. Ye, “Error Bounds Analysis of De-Embedded Results in 2X-Thru De-Embedding Methods,” in Proc. IEEE Int. Symp. on EMC and SI/PI (EMCSI), Washington, DC, 2017.
[10] IEEE P370 Standard, Available: opensource.ieee.org; www.mathworks.com.
[11] C.-C. Chou and J.-H. Hsu, “An Impedance-Corrected 2X-Thru Calibration,” IEEE Microwave and Wireless Technology Letters, vol. 33, no. 12, Dec. 2023.
[12] J. J. Ellison and S. S. Agili, “Impedance Corrected De-Embedding,” IEEE Electromagnetic Compatibility Magazine, vol. 11, no. 3, 3rd Quarter 2022.
[13] M.-P. Dubuisson and A. K. Jain, “A Modified Hausdorff Distance for Object Matching,” in Proc. Int. Conf. on Pattern Recognition (ICPR), Jerusalem, Israel, Oct. 1994.
[14] K. E. Mattar, D. G. Watters, and M. E. Brodwin, “Influence of Wall Contacts on Measured Complex Permittivity Spectra at Coaxial Line Frequencies,” IEEE Transactions on Microwave Theory and Techniques, vol. 39, no. 3, Mar. 1991.
[15] Röchling Glastic Composites, “HT200_Datenblatt2023,” Available: www.bmf3d.com/de/.